Acta Pharmacologica Sinica

www.nature.com/aps

ARTICLE

Diterbutyl phthalate attenuates osteoarthritis in ACLT mice via suppressing ERK/c-fos/NFATc1 pathway, and subsequently inhibiting subchondral osteoclast fusion

Chao Fang[1], Jia-wei Guo[1], Ya-jun Wang[1], Xiao-qun Li[1], Hao Zhang[1], Jin Cui[1], Yan Hu[1], Ying-ying Jing[2], Xiao Chen[1,3] and Jia-can Su[1,2,4]

Osteoarthritis (OA) is the most common arthritis with a rapidly increasing prevalence. Disease progression is irreversible, and there is no curative therapy available. During OA onset, abnormal mechanical loading leads to excessive osteoclastogenesis and bone resorption in subchondral bone, causing a rapid subchondral bone turnover, cyst formation, sclerosis, and finally, articular cartilage degeneration. Moreover, osteoclast-mediated angiogenesis and sensory innervation in subchondral bone result in abnormal vascularization and OA pain. The traditional Chinese medicine *Panax notoginseng* (PN; Sanqi) has long been used in treatment of bone diseases including osteoporosis, bone fracture, and OA. In this study we established two-dimensional/bone marrow mononuclear cell/cell membrane chromatography/time of flight mass spectrometry (2D/BMMC/CMC/TOFMS) technique and discovered that diterbutyl phthalate (DP) was the active constituent in PN inhibiting osteoclastogenesis. Then we explored the therapeutic effect of DP in an OA mouse model with anterior cruciate ligament transaction (ACLT). After ACLT was conducted, the mice received DP (5 mg·kg^{-1}·d^{-1}, ip) for 8 weeks. Whole knee joint tissues of the right limb were harvested at weeks 2, 4, and 8 for analysis. We showed that DP administration impeded overactivated osteoclastogenesis in subchondral bone and ameliorated articular cartilage deterioration. DP administration blunted aberrant H-type vessel formation in subchondral bone marrow and alleviated OA pain assessed in Von Frey test and thermal plantar test. In RANKL-induced RAW264.7 cells in vitro, DP (20 μM) retarded osteoclastogenesis by suppressing osteoclast fusion through inhibition of the ERK/c-fos/NFATc1 pathway. DP treatment also downregulated the expression of dendritic cell-specific transmembrane protein (DC-STAMP) and d2 isoform of the vacuolar (H+) ATPase V0 domain (Atp6v0d2) in the cells. In conclusion, we demonstrate that DP prevents OA progression by inhibiting abnormal osteoclastogenesis and associated angiogenesis and neurogenesis in subchondral bone.

Keywords: osteoarthritis; *Panax notoginseng*; diterbutyl phthalate; osteoclastogenesis; subchondral bone; ERK/c-fos/NFATc1 pathway; two-dimensional cell membrane chromatography (2D/CMC); ACLT mice

Acta Pharmacologica Sinica (2022) 43:1299–1310; https://doi.org/10.1038/s41401-021-00747-9

INTRODUCTION

Osteoarthritis (OA), a chronic and whole joint degenerative disorder characterized by an irreversible progression, is an age-related disease with a high incidence and an increasing global prevalence, resulting in joint stiffness, pain, and disability [1]. Currently, it is estimated that 250 million people worldwide suffer from symptomatic OA [2]. By 2030, this number will be 400 million [3]. In China, knee OA affects approximately 10% of females and 6% of males [4].

OA is characterized by worn articular cartilage, synovial lesions, capsule contracture, osteophyte formation, and subchondral bone marrow lesions [5, 6]. To date, multiple pharmaceutical strategies for OA, including protease inhibitors, anti-inflammatory therapies, stem cell administrations, and biologic agents, have been investigated, but the efficacy and safety of these therapies are still ambiguous [7]. Clinically, apart from terminal-stage surgical arthroplasty, no therapeutic strategies to rescue OA progression are available [8].

Subchondral bone is crucial for OA onset [9–11]. Articular cartilage and subchondral bone constitute a mechanical and functional unit in which the stiffness intensity of subchondral bone provides a supporting basis for articular cartilage and dissipates severe loadings applied to the weight-bearing joints [12]. During OA onset, obesity and muscle atrophy during aging or traumatic ligament damage result in abnormal mechanical loads on joints [13, 14]. Matrix-embedded osteocytes sense mechanical alterations and orchestrate osteoclast differentiation and function, leading to excessive activation of osteoclastogenesis in subchondral bone and subsequent bone resorption [15]. Ample evidence indicates that osteoclastic bone resorption is abnormally upregulated during the initial stage of OA, leading to a rapid subchondral bone turnover [16–18]. H-type vessels, characterized by CD31^{high}

[1]Department of Orthopedics Trauma, Shanghai Changhai Hospital, Naval Medical University, Shanghai 200433, China; [2]Institute of Translational Medicine, Shanghai University, Shanghai 201901, China; [3]Department of Chemistry, Fudan University, Shanghai 200433, China and [4]Shanghai Clinical Research Center for Aging and Medicine, Shanghai 200040, China
Correspondence: Ying-ying Jing (jingy4172@shu.edu.cn) or Xiao Chen (sirchenxiao@126.com) or Jia-can Su (drsujiacan@163.com)
These authors contributed equally: Chao Fang, Jia-wei Guo

Received: 26 January 2021 Accepted: 17 July 2021
Published online: 11 August 2021

and endomucin^{high} (CD31^{hi} EMCN^{hi}) levels, which are closely associated with bone remodeling, exacerbate the cartilage erosion in OA [19, 20]. Netrin-1, derived from osteoclasts, mediates the infiltration of sensory nerves into subchondral bone, followed by hyperalgesia and pain in OA mice [21–23]. Therefore, targeting overactivated osteoclasts in subchondral bone serves as an effective approach for OA treatment [24].

Panax notoginseng (PN; Sanqi), a natural plant, has various biological properties, including promoting fracture healing [25], anti-inflammation [26], neuroprotection [27], and anti-osteoporosis [28]. Studies have shown that PN exerts a positive pain relief influence on OA [29, 30]. Based on our previous studies, we screened an active component from PN using the two-dimensional/bone marrow mononuclear cell/cell membrane chromatography/time of flight mass spectrometry (2D/BMMC/CMC/TOFMS) technique [31–33]. Theoretically, components with a strong affinity for the BMMC membrane could be potentially effective in regulating osteoclast differentiation.

In this study, we find that diterbutyl phthalate (DP), an active constituent screened from PN using the 2D/BMMC/CMC/TOFMS system, inhibits osteoclastogenesis. DP prevents OA progression in anterior cruciate ligament transaction (ACLT) mice by inhibiting abnormal osteoclastogenesis as well as the associated angiogenesis and neurogenesis in subchondral bone. For mechanisms, we demonstrate that DP blocks osteoclast fusion.

MATERIALS AND METHODS

Identifying active constituents

Bone marrow mononuclear cells (BMMCs) were extracted from male C57BL/6J mice (4 weeks old) by flushing the bone marrow of bilateral femurs. PN (50 g) was dissolved in 50% ethanol, converted into a 1.0 g/mL concentrated solution, and then incubated with BMMCs. The 2D/BMMC/CMC/TOFMS assay was employed to evaluate the binding capability of PN components to BMMC membranes. Compound data were recorded by an Agilent MassHunter Workstation (Agilent Technologies, Palo Alto, CA, USA) and translated into written code using Visual Basic 6.0 software (Microsoft, Redmond, WA, USA). MATLAB software (MathWorks, USA) was utilized to draw three-dimensional graphics. Compounds with a sustained retention time were identified as active ingredients for inhibiting osteoclastogenesis.

Reagents and antibodies

DP (ST1999010.1 ML) was obtained from Standard Company (Shanghai, China). Mouse soluble receptor activator of nuclear factor-κB ligand (RANKL) (462-TEC) and macrophage-colony stimulating factor (M-CSF) (416-ML) were purchased from R&D Systems (Minneapolis, MN, USA). Paraformaldehyde (PFA) (P1110-100) and ethylenediaminetetraacetic acid (EDTA) (E1171) were supplied by Solarbio (Beijing, China). Cell Counting Kit-8 (CCK-8) (C0038) was supplied by Beyotime (Shanghai, China). Tartrate-resistant acid phosphatase (TRAP) kit (387A-1KT) was provided by Sigma-Aldrich (St. Louis, MO, USA). Ceramide C6 (860704) was purchased from Avanti Polar Lipids (Alabaster, AL, USA).

Cell viability assay

BMMCs (1×10^4/well, 100 μL) and RAW264.7 cells (5×10^3/well, 100 μL) were cultured separately in 96-well plates and then incubated with DP at incremental concentrations for 48 h. Cells were washed with phosphate-buffered saline (PBS) twice and then cultured with CCK-8 solution (10 μL) for 2 h (37 °C, 5% CO_2). The absorbance at 450 nm was then measured by enzyme-linked immunosorbent assay.

Osteoclastogenesis assay

BMMCs were incubated on a petri dish in alpha-modified minimal essential medium containing 10% fetal bovine serum (FBS), 1% penicillin, 1% streptomycin, and M-CSF (30 ng/mL) overnight (37 °C, 5% CO_2). Nonadherent cells were extracted and seeded into 96-well plates (1×10^4/well, 100 μL) with M-CSF (30 ng/mL) for 2 days. For osteoclastogenesis, cells were incubated with M-CSF (30 ng/mL) and RANKL (100 ng/mL) in the presence or absence of the indicated DP for 5 days. Next, cells were washed with PBS twice and fixed in 4% PFA for 30 min, then TRAP staining was conducted, and TRAP-positive multinucleated cells were quantified.

RAW264.7 cells were seeded on a petri dish in Dulbecco's modified Eagle's medium supplemented with 10% FBS, 1% penicillin, and 1% streptomycin for 24 h (37 °C, 5% CO_2). For osteoclastogenesis, adherent cells were washed with PBS twice and plated in 96-well plates (5×10^3/well, 100 μL) with RANKL (100 ng/mL) in the presence or absence of different concentrations of DP for 7 days, then TRAP assay was performed.

Osteoclast fusion analysis

After RAW264.7 cells were incubated with RANKL (100 ng/mL) with or without different doses of DP for 3 days, cell membranes were stained with red Dil (Fushen, Shanghai, China), and cell nuclei were dyed blue with Hoechst (Beyotime, Shanghai, China). Labeled cells were imaged using a fluorescence microscope (Olympus BX53). ImageJ (NIH, Bethesda, MD, USA) was employed to quantify the rate of membrane fusion (%).

ACLT-induced OA mouse models

Male C57BL/6J mice (8 weeks old) were obtained from Weitonglihua Corporation (Beijing, China). Mouse experiments were performed in a specific pathogen-free laboratory. All operational procedures conformed to the standards and guidelines of the Bioethics Committee of Changhai Hospital (SYXK 2015-0017). Mice weighing between 20 and 22 g were maintained at temperatures between 20 and 24 °C with a 12 h light–dark cycle and relative humidity ranging from 50% to 60%. Water and food were available throughout the entire duration of the experiment. According to the standard protocols elaborated previously [34], OA mouse models were generated with an ACLT operation to mimic mechanical instability. Specifically, after intraperitoneal anesthesia with 5% chloral hydrate, mice underwent a longitudinal cutaneous incision in the right knee. The ACL was transected under a surgical microscope with an ophthalmic scalpel. Alendronate (ALN) was used as a positive control in relative to DP [35–37]. Twenty-four hours later, mice were randomly assigned to four groups: sham (stitching the right knee incision after opening the knee capsule and treated with normal saline), ACLT (ACLT mice injected with normal saline), DP (ACLT mice injected with DP), and ALN (ACLT mice injected with ALN). Over the next 8 weeks, mice in DP group were intraperitoneally administered DP (5 mg·kg^{-1}·d^{-1}), mice in the ALN group (1 mg·kg^{-1}) were injected intraperitoneally three times per week [21], and mice in the sham and ACLT groups simultaneously received the same volume of normal saline. Whole knee joint tissues of the right limb were harvested after euthanasia of mice at weeks 2, 4, and 8 for further analysis.

Western blotting

Cultured cells were lysed with 200 μL RIPA buffer containing 1% phenylmethylsulfonyl fluoride. Western blotting was conducted according to standard protocols [38]. Antibodies against Cathepsin K (CTSK) (DF6614), Netrin-1 (DF8579), phospho-ERK1/2 (AF1015), ERK1/2 (AF0155), c-fos (AF0132), and NFATc1 (DF6446) were obtained from Affinity (Cincinnati, OH, USA). Antibodies against Atp6v0d2 (bs-12548R) and DC-STAMP (bs-8250R) were purchased from Bioss (Beijing, China). After incubation with primary antibodies against CTSK (1:1000), Netrin-1 (1:1000), phospho-ERK1/2 (1:1000), ERK1/2 (1:2000), c-fos (1:1000), NFATc1 (1:1000), Atp6v0d2 (1:500), and DC-STAMP (1:500) overnight (4 °C),

samples were incubated with secondary antibodies. Protein bands were visualized using a chemiluminescence apparatus (Bio-Rad).

Histological analysis

Mouse knee joint tissues were harvested and fixed in 4% PFA for 48 h, followed by decalcification in 10% EDTA for 2 weeks. Then, samples were embedded in paraffin and serially sectioned (4-μm thickness) in the sagittal view of the medial compartment of the knee joint. Each knee was embedded in the same orientation. Next, hematoxylin and eosin (H&E), Safranin O and fast green, and TRAP staining were performed following standard protocols [39]. The knee joint area was imaged under a light microscope (Olympus BX53). The tidemark line labels the boundary between hyaline cartilage (HC) and calcified cartilage (CC). H&E staining with 20× modified image was used for measurement of the thickness of HC and CC. The Osteoarthritis Research Society International score (OARSI) was employed to evaluate and quantify the degradation of tibial plateau cartilage as previously described [40].

Immunochemistry and immunofluorescence analysis

Antibodies against aggrecan (ACAN) (GB11373) and collagen 2 (Col-2) (GB11021) were bought from Servicebio (Wuhan, China). Antibodies against Lubricin (ab28484), matrix metalloproteinase (MMP)-13 (ab219620), collagen X (Col-X) (ab260040), TRAP (ab191406), CD31 (ab182981), endomucin (EMCN) (ab106100), MMP-2 (ab97779), and calcitonin gene-related peptide (CGRP) (ab36001) were obtained from Abcam (Cambridge, UK). Sagittal sections of the knee joint medial compartment were incubated using primary antibodies against Lubricin (1:50), MMP-13 (1:400), Col-X (1:50), ACAN (1:500), Col-2 (1:200), TRAP (1:800), CD31 (1:4000), EMCN (1:200), MMP-2 (1:1000), CGRP (1:2000), and Netrin-1 (1:100) overnight (4 °C). Immunochemistry and immunofluorescence were conducted according to standard operating procedures [41]. Histomorphometry detection was applied to a region of the tibial subchondral bone. The number of positively stained cells in subchondral bone and cartilage was quantified using ImageJ.

After RAW264.7 cells were incubated with RANKL (100 ng/mL) in the presence or absence of the indicated DP, cells were washed with PBS twice, fixed with 4% PFA, and blocked in 5% BSA at room temperature. Next, cells were successively incubated with NFATc1 antibody (1:50) overnight (4 °C) and secondary antibody (1:100) for 1 h. Cell nuclei were stained with Hoechst for 15 min. Finally, NFATc1 nuclear translocation was visualized using a fluorescence microscope (Olympus BX53).

Micro-CT analysis

Knee joints were scanned by microcomputed tomography (micro-CT; Bruker skyscan1176, USA) at 9 μm resolution, 50 kV X-ray voltage, and 60 μA current. After a scanned image was imported into Data-Viewer software (version 1.5), the volume of interest was selected and saved as collected data, which was further analyzed using CT-An software (version 1.15). The three-dimensional image of the sagittal plane of the tibial plateau structure was reconstructed using CT-Vol software (version 1.14). The following structural parameters of subchondral bone were measured in scanned images: bone volume/tissue volume (BV/TV, %), trabecular separation (Tb. Sp, μm) and subchondral bone plate thickness (SBP. Th, μm).

Microangiography

After mice were anesthetized, cardiac perfusion was performed by left venipuncture, and the systemic circulation was successively perfused with PBS containing heparin sodium (125 U/mL), 10% PFA, and the angiography agent (Microphil MV-120, Flow-Tech). To achieve a viscosity level appropriate for microcirculation injection, volume mixing requires 50% of the diluent for each 40% of the compound, and this mixture is catalyzed with 5% (by weight) curing agent. The working time was 20 min after the addition of a curing agent. After angiography was performed, mice were stored overnight (4 °C), and then specimens were dissected and fixed in 4% PFA for 48 h, followed by decalcification in 10% EDTA for 2 weeks. The procedure of knee joint scanning by micro-CT is described in the preceding paragraph.

Von Frey test

Von Frey hairs (Touch test, USA) were employed to measure the 50% paw withdrawal threshold (50% PWT). Briefly, mice were placed in cages with metal mesh bottoms for 20 min to adapt them to the testing environment (stopping exploratory behavior and being still) [42]. According to the baseline confirmed before the test, Von Frey filaments implied in this test were set as the following serial forces (gram = 0.04, 0.07, 0.16, 0.4, 0.6, 1.0, 1.4, 2.0), and 2.0 g was set as the cutoff threshold. Mechanical allodynia was tested according to the up-down method of Dixon [43] and was conducted at the same time every day. The filament was started from the filament of 0.4 g and acupunctured beneath the middle plantar area of the right hind paw until it bent as a "S" shape for 3–5 s. If there was a negative response (written as "o"), the next higher force was applied. If there was a positive response (written as "x"), the next lower force was adopted. The sequence of outcomes was recorded. After the first difference of response was recorded ("ox" or "xo"), four extra tests were performed to guarantee at least six measurements in total. The interval between adjacent stimuli was at least 5 min. Fifty percent PWT was calculated using the following formula: $10^{[Xf+k\delta]}/10^4$, where Xf is the value (in log units) of the last filament used, k is determined by reference to the response pattern (modified from Dixon), and δ is a constant (in log units) from the standard deviation (SD) of serial force.

Thermal plantar test

Paw withdrawal latency (PWL) was assessed by the thermal plantar test (II TC Life Science Model 390, USA) as previously reported [44]. Prior to the experiment, the device was calibrated to present a PWL of approximately 10 s on average, and the cutoff latency was set at 20 s to avoid tissue injury. Mice were placed in cages with glass bottoms for 20 min to accustom themselves to the environment. A 40 W infrared heat source was located below the middle plantar area of the right hind paw through the heat-conducting glass floor. We recorded the time taken from the commencement of stimulus to paw withdrawal. Tests were conducted three times with 5 min intervals, and the mean value was recorded as the nociceptive latency.

Statistical analysis

Data in this study are presented as the mean ± SD. Comparisons among three groups were performed by one-way analysis of variance. GraphPad Prism 6.07 (GraphPad Software, San Diego, CA, USA) was utilized to finish the statistical analysis. $P < 0.05$ and $P < 0.01$ were considered to show the level of statistical significance.

RESULTS

DP is the active constituent identified from PN

Both clinical and basic studies indicate that PN could alleviate OA symptoms and prevent OA progression [29, 30]. Nevertheless, the mechanism remains unclear. Targeting subchondral bone overactivated osteoclasts in early OA could prevent disease progression [17, 21]. Therefore, we employed the two-dimensional cell membrane chromatography (2D/CMC), a highly sensitive and high-throughput biological chromatography to screen active components from PN as previously mentioned [33, 45]. Compounds with a sustained retention time were

regarded as active ingredients. Here, DP ($C_{16}H_{22}O_4$) showed a strong binding affinity for BMMC membranes by 2D/BMMC/CMC/TOFMS. The response of TOFMS showed that DP had a strong retention behavior, reaching a peak at 5 min and maintaining high levels for 20 min (Supplementary Fig. S1). This result illustrates that DP is an active monomer screened from PN.

DP attenuates articular cartilage degradation in ACLT mice

During OA, the integrity of articular cartilage undergoes significant pathological alterations in morphology and composition. The tidemark replication results in the expansion of the underlying CC to replace the overlying HC. Proteoglycan loss in articular cartilage features OA progression. To investigate the effect of DP on ACLT-induced articular cartilage degeneration, H&E staining was performed and revealed that the thickness of CC underwent a remarkable increase from 2 to 8 weeks after ACLT, implying a progressive disruption of articular cartilage. In contrast, these alterations were prevented in the DP-treated group in relative to ACLT group. Simultaneously, the decreased HC thickness after surgery was significantly maintained in DP group. No significant differences in CC or HC thickness were observed between sham and DP groups at 2, 4, and 8 weeks after ACLT (Fig. 1a, c, d).

In parallel, Safranin O staining showed that there were local fibrillations with the loss of proteoglycans in the surface region of articular cartilage in ACLT group at 4 weeks after the ACLT, suggesting the breakdown of collagen network. The decreased proteoglycan levels in ACLT mice were notably preserved by DP to a level comparable to that of sham group. At 8 weeks post ACLT, osteophyte formation was observed at the margin of the joint, this phenotype was accompanied by deeper cracks in articular cartilage, indicating OA progression. In contrast, the content of proteoglycans and the normal microstructure of articular cartilage

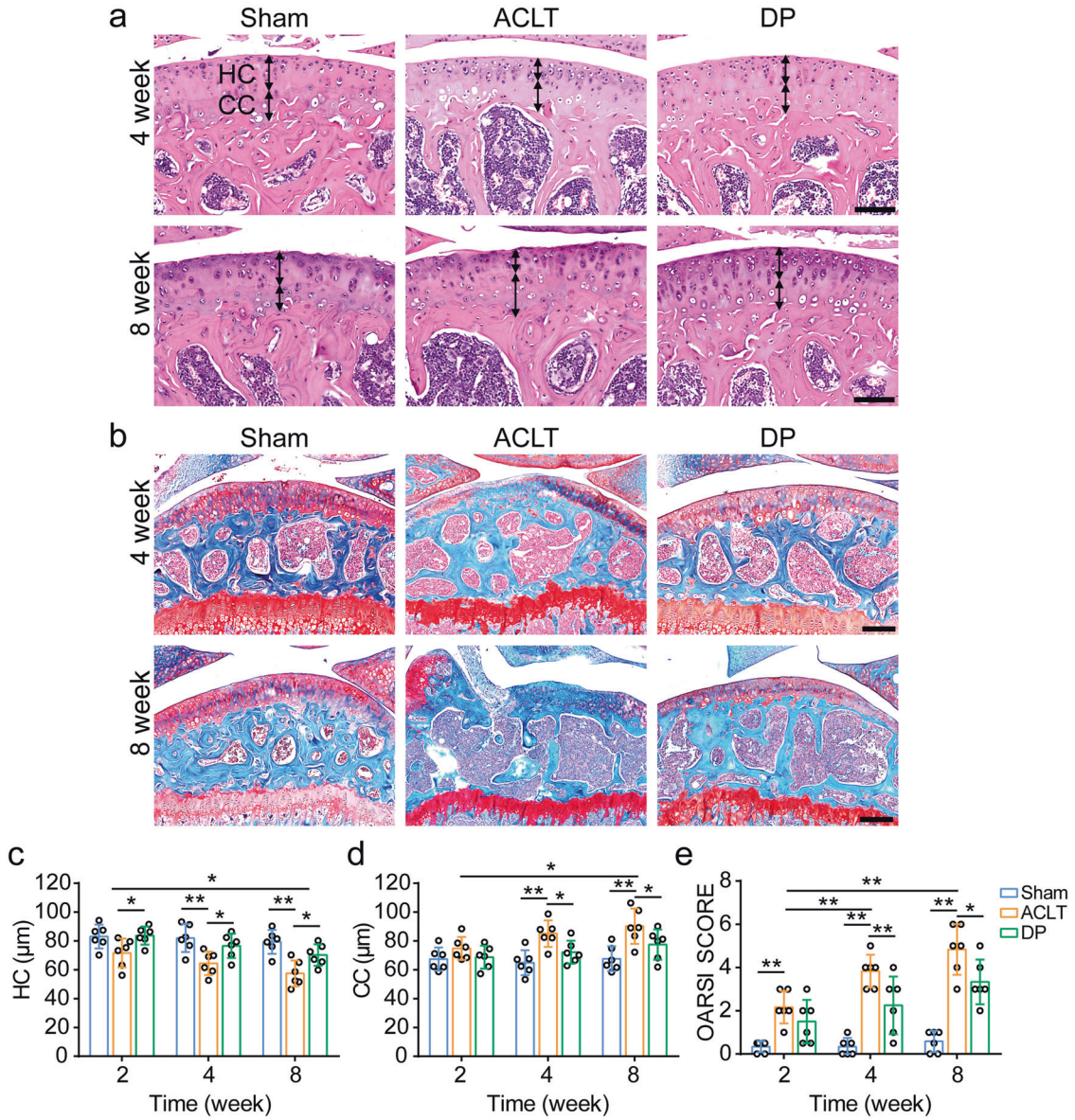

Fig. 1 DP attenuates articular cartilage degradation after ACLT. a, **b** H&E staining (**a**) and Safranin O staining (**b**) at 4 and 8 weeks after ACLT. HC and CC thickness are labeled with double-headed arrows. Scale bar = 100 μm. **c**, **d** Quantitative analysis of thickness of HC (**c**) and CC (**d**) in three groups. **e** Osteoarthritis Research Society International (OARSI) histology scoring of tibial plateau articular cartilage after surgery in three groups. Sham sham operation, ACLT ACLT mice treated with normal saline, DP ACLT mice treated with DP. *$P < 0.05$ and **$P < 0.01$ compared with ACLT group or as denoted by bar.

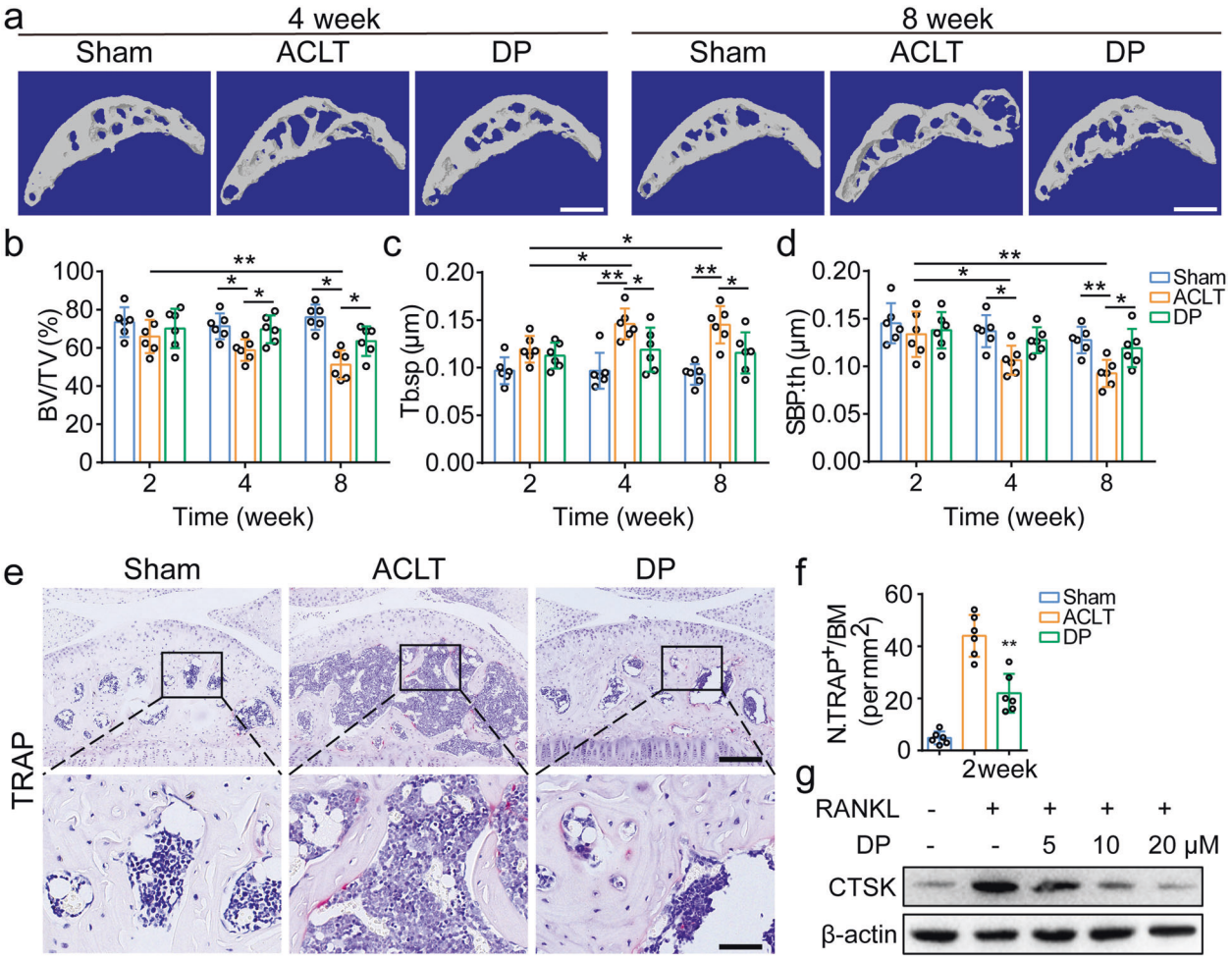

Fig. 2 DP preserves subchondral bone microstructure after ACLT. a Three-dimensional images of the sagittal plane of medial tibial subchondral bone structure at 4 and 8 weeks after operation. Scale bar = 500 μm. **b**–**d** Micro-CT quantitative analysis of tibial subchondral bone of bone volume/tissue volume (BV/TV, %) (**b**), trabecular separation (Tb. Sp, μm) (**c**), and subchondral bone plate thickness (SBP. Th, μm) (**d**). **e**, **f** TRAP staining (**e**) and quantitative analysis (**f**) of TRAP-positive osteoclast in subchondral bone marrow at 2 weeks post operation. Scale bar = 200 μm (top). Scale bar = 50 μm (bottom). **g** Western blotting assay of CTSK in cultured RAW264.7 cells induced for 7 days in the absence or presence of RANKL, treated with different concentrations of DP (5, 10, and 20 μM). Sham sham operation, ACLT ACLT mice treated with normal saline, DP ACLT mice treated with DP. $^{*}P < 0.05$ and $^{**}P < 0.01$ compared with ACLT group or as denoted by bar.

were substantially preserved by DP treatment in relative to ACLT group (Fig. 1b). The OARSI system was adopted to evaluate the pathological damage of articular cartilage [40]. Compared to ACLT group, DP significantly improved the OARSI scores, which remained at low levels in sham group (Fig. 1e).

In this part, to further verify the therapeutic effect of DP on cartilage degradation in OA, ALN was selected as a positive control drug, which exerted inhibitory effect on osteoclastic bone resorption and attenuated OA progression as previously reported [14, 36, 46]. H&E staining showed that ALN impeded the increased thickness of CC in articular cartilage after ACLT. Conversely, the ACLT-associated reduced thickness of HC was improved by ALN (Supplementary Fig. S2a, c, d). It was noted that the ACLT-induced proteoglycan loss and osteophyte formation were also prevented by ALN as assessed by Safranin O staining (Supplementary Fig. S2b). Furthermore, the OARSI score showed no significant differences of the protective influence on cartilage degradation in ACLT mice between DP and ALN group (Supplementary Fig. S2e). Hence, these results illustrated that ALN exerted a positive effect comparable to that of DP.

Immunohistochemistry staining illustrated that Lubricin, ACAN, and Col-2 were significantly decreased in ACLT mice but were preserved by DP treatment. In contrast, the high expression of joint degradation indexes (MMP-13 and Col-X) was decreased by DP intervention, as shown by immunofluorescence staining (Supplementary Fig. S3). Collectively, these findings indicate that DP prevents articular cartilage degradation and abrasion after ACLT.

DP suppresses overactivated osteoclastogenesis in subchondral bone

To identify the role of DP in osteoclastogenesis in subchondral bone, we assessed the effect of DP on microstructural changes in subchondral bone in the proximal tibia using micro-CT scanning. For micro-CT analysis, BV/TV refers to the common parameter for the description of cancellous bone mass in subchondral bone. Tb. Sp is adopted to estimate the connectivity and microstructure of the subchondral trabecular bone. Higher Tb. Sp means lower resistance to deformation. SBP. Th is used to reflect the bone plate thickness and is the major indicator of the mechanic strength of subchondral bone. From 2 to 8 weeks post operation, tibial subchondral BV/TV and SBP. Th were decreased, and Tb. Sp was increased in ACLT mice in relative to sham group, indicating increased osteoclastic bone

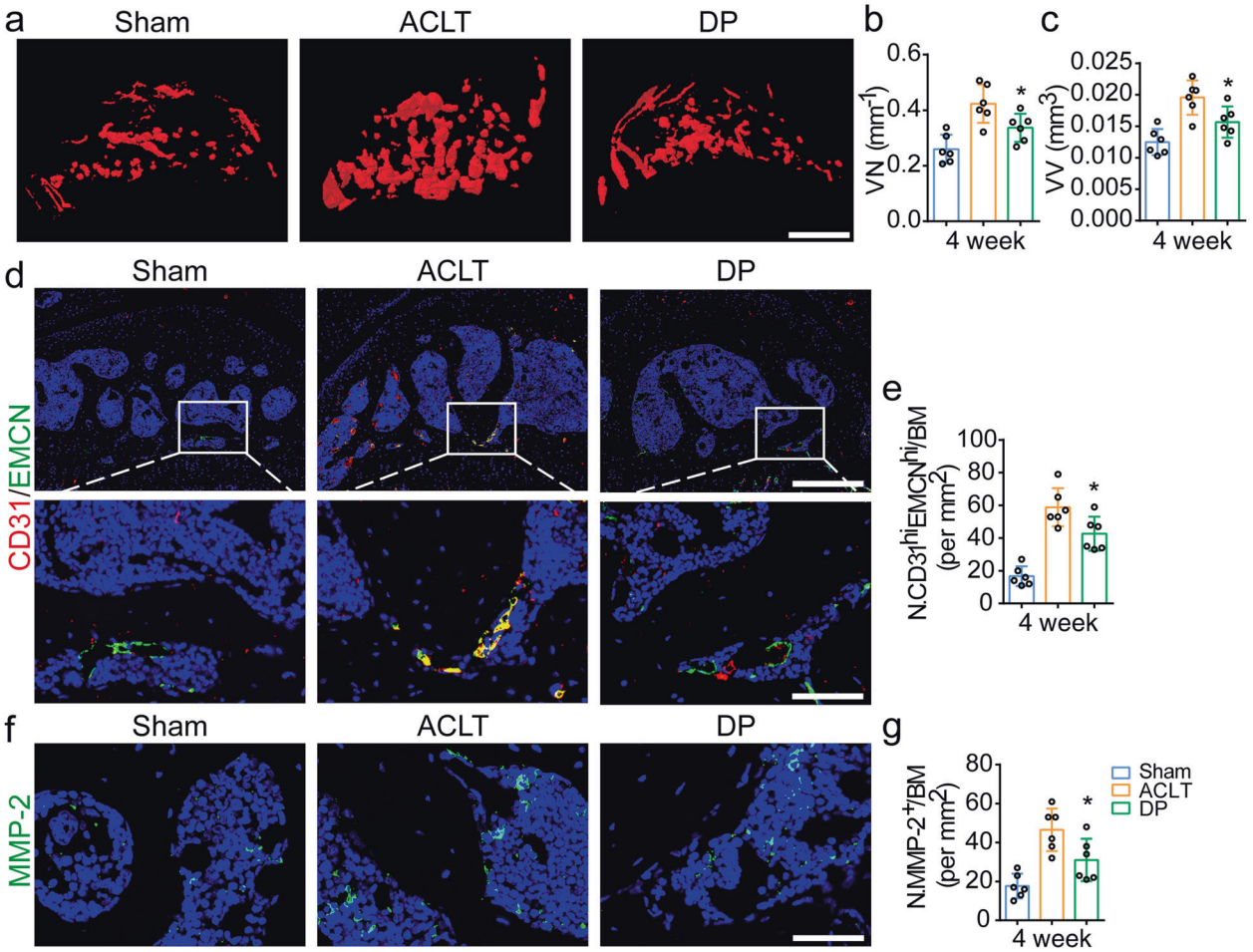

Fig. 3 DP represses abnormal angiogenesis in subchondral bone. a Three-dimensional image of the sagittal plane of CT-based microangiography in medial tibial subchondral bone at 4 weeks post operation. Scale bar = 500 μm. **b**, **c** Quantification of VN (**b**) and VV (**c**) in three groups. **d**, **e** Representative immunofluorescence double staining (**d**) and quantification (**e**) of CD31 (red) and EMCN (green) positive cells in subchondral bone marrow at 4 weeks after surgery. Scale bar = 200 μm (top). Scale bar = 50 μm (bottom). **f**, **g** Immunofluorescence staining (**f**) and quantification (**g**) of MMP-2 positive cells in subchondral bone marrow at 4 weeks after surgery. Scale bar = 50 μm. Sham sham operation, ACLT ACLT mice treated with normal saline, DP ACLT mice treated with DP. *$P < 0.05$ compared with ACLT group.

resorption and marked bone loss. Micro-CT indicated that the elevated bone turnover rate exacerbates the porosity of subchondral bone trabeculae, as quantitatively shown by BV/TV and Tb. Sp. Moreover, compared to sham group, SBP. Th in ACLT group was decreased with more trabecular cracks, implying structural network damage in subchondral bone as a result of overactivated osteoclastogenesis. These alterations of BV/TV, Tb. Sp and SBP. Th were associated with decreased stiffness in the bone tissue and weakness in bone. Notably, these indexes were significantly normalized by DP to a level comparable to that of sham group. No significant differences were observed in BV/TV or SBP. Th and Tb. Sp between DP-treated mice and sham mice, indicating that the mechanical strength of subchondral bone was maintained by DP intervention. The subchondral bone in DP group was more resistant to deformation, preventing rapid OA development (Fig. 2a–d).

In addition, compared to sham group, the number of TRAP-positive osteoclasts was significantly increased in ACLT group 2 weeks after surgery in subchondral bone, which was diminished by DP intervention, further suggesting the anti-osteoclastogenesis effect of DP in vivo (Fig. 2e, f). CTSK is a dominant osteolytic protease in mature osteoclasts. Western blotting showed that CTSK was upregulated after RANKL induction but was notably repressed in response to DP intervention (5, 10, or 20 μM) in vitro, and this suppressive effect was dose-dependent (Fig. 2g). Taken together, the data support that the ACLT-induced mouse model leads to overactivated osteoclastogenesis and bone resorption in subchondral bone, whereas this pathological process is markedly prevented by DP.

DP inhibits aberrant blood vessel formation in subchondral bone Abnormal angiogenesis in subchondral bone is one hallmark of OA [47]. To determine the role of DP in subchondral bone angiogenesis after ACLT, microangiography was adopted, and results showed that both vessel number (VN) and vessel volume (VV) were significantly increased in ACLT group and were decreased by DP treatment in subchondral bone (Fig. 3a–c). Next, we examined whether DP had an inhibitory influence on H-type vessels using double immunofluorescence staining for CD31 and EMCN. Results indicated that number of $CD31^{hi}$ $EMCN^{hi}$ blood vessels was aberrantly increased in ACLT mice and inhibited after DP treatment, which was comparable to that observed in sham mice, implying that the type-H angiogenesis was increased in subchondral bone in ACLT group but was notably impeded by DP treatment (Fig. 3d, e). Immunofluorescence staining showed that MMP-2 [48], a well-established factor attributed to abnormal blood

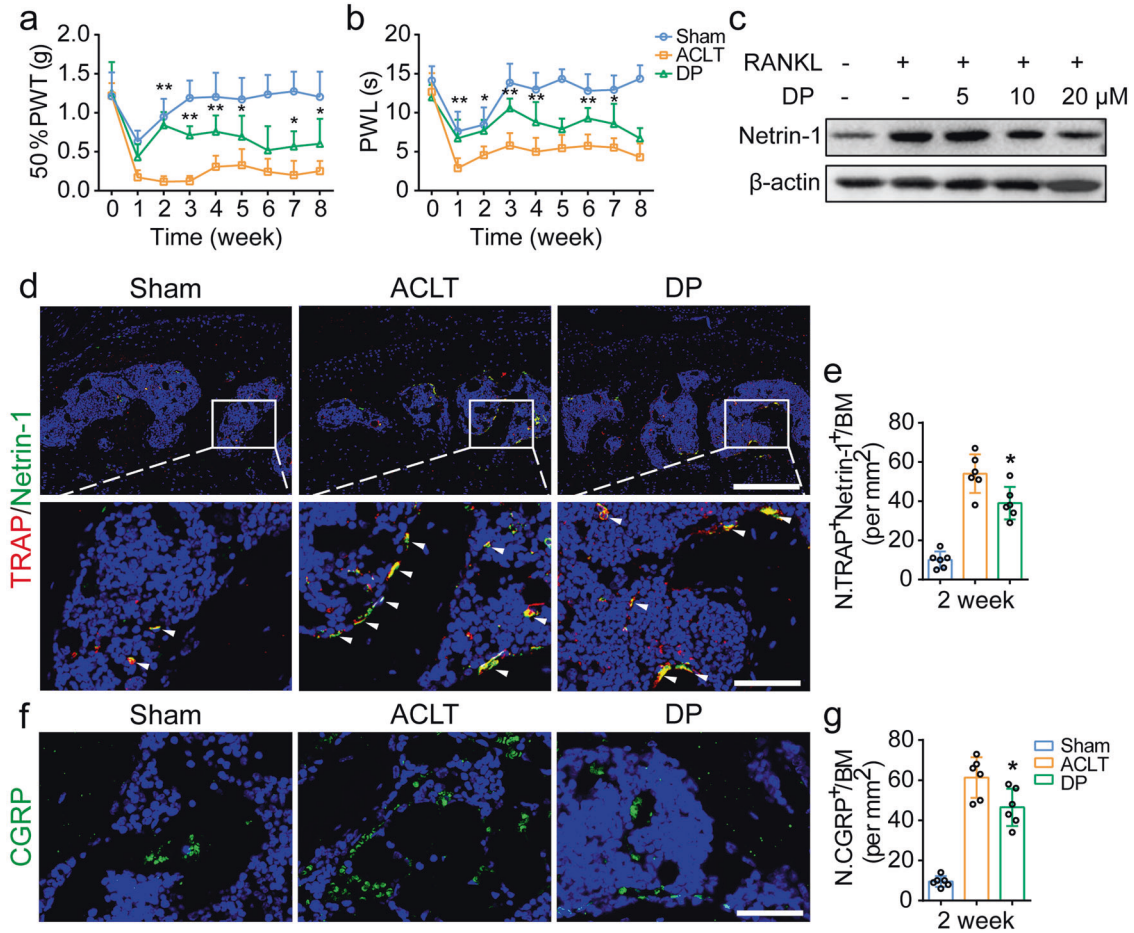

Fig. 4 DP alleviates OA-associated pain. a, **b** Pain-related behaviors and quantitative analysis of 50% PWT (**a**) and PWL (**b**) from 0 to 8 weeks. **c** Western blotting assay of netrin-1 in cultured RAW264.7 cells induced for 7 days in the absence or presence of RANKL, treated with different concentrations of DP (5, 10, and 20 μM). **d**, **e** Representative immunofluorescence double staining (**d**) and quantification (**e**) of TRAP (red) and netrin-1 (green) positive cells in subchondral bone marrow at 2 weeks post operation. Scale bar = 200 μm (top). Scale bar = 50 μm (bottom). **f**, **g** Immunofluorescence staining (**f**) and quantification (**g**) of CGRP positive cells in subchondral bone at 2 weeks after surgery. Scale bar = 50 μm. Sham sham operation, ACLT ACLT mice treated with normal saline, DP ACLT mice treated with DP. $^{*}P < 0.05$ and $^{**}P < 0.01$ compared with ACLT group.

vessel formation, was also apparently abolished by DP compared to that in ACLT group, further suggesting the anti-angiogenic effect of DP (Fig. 3f, g). In summary, these results indicate that DP inhibits excessive angiogenesis in subchondral bone during OA progression.

DP relieves pain in ACLT mice

To demonstrate whether DP alleviates osteoclast-mediated pain in ACLT mice. First, Von Frey tests and thermal plantar tests were performed to assess whether DP influences pain-related behavioral phenotypes. We found that there was a tremendous alteration of nociceptive reaction in ACLT mice compared to those in sham group from the first week after surgery. However, this exacerbated ACLT-mediated pain was partly ameliorated after DP treatment, suggesting that OA-associated mechanical and thermal pain was alleviated by DP (Fig. 4a, b). Western blotting illustrated that the increased expression levels of netrin-1 in RANKL-induced osteoclastogenesis were dampened by DP (5, 10, or 20 μM) in vitro in a dose-dependent manner (Fig. 4c). Netrin-1 secreted from osteoclasts plays an inductive role in OA-related pain by promoting axonal growth [21]. In line with the behavioral results, immunofluorescence staining indicated that after ACLT, the number of $TRAP^{+}$/Netrin-1^{+} osteoclasts in subchondral bone was significantly increased and was decreased with DP treatment (Fig. 4d, e). As a result, staining of CGRP in subchondral bone marrow showed that DP significantly inhibited the increased CGRP positive sensory innervation in ACLT mice (Fig. 4f, g). Taken together, these findings verify that excessive stimulation of netrin-1 secreted by osteoclasts and CGRP induced by OA is retarded by DP, which apparently attenuates osteoclast-induced OA pain.

DP inhibits osteoclastogenesis in vitro

To further determine the effect of DP on osteoclastogenesis in vitro. First, we explored the noncytotoxic concentration of DP (<20 μM) by CCK-8 assay. Results showed that DP exerted no significant toxicological effect on BMMC and RAW264.7 cells proliferation when its concentration was below 20 μM, while DP with those concentrations over 50 μM presented inhibitory effect on cells proliferation (Supplementary Fig. S4). Next, the TRAP assay was performed and indicated that RANKL-stimulated osteoclastogenesis from BMMCs and RAW264.7 cells was significantly compromised by DP treatment (5, 10, or 20 μM) in a dose-dependent manner (Fig. 5a–d). Specifically, differentiation of osteoclasts was slightly suppressed by DP at a low concentration (5 μM). As the concentration rose from 10 to

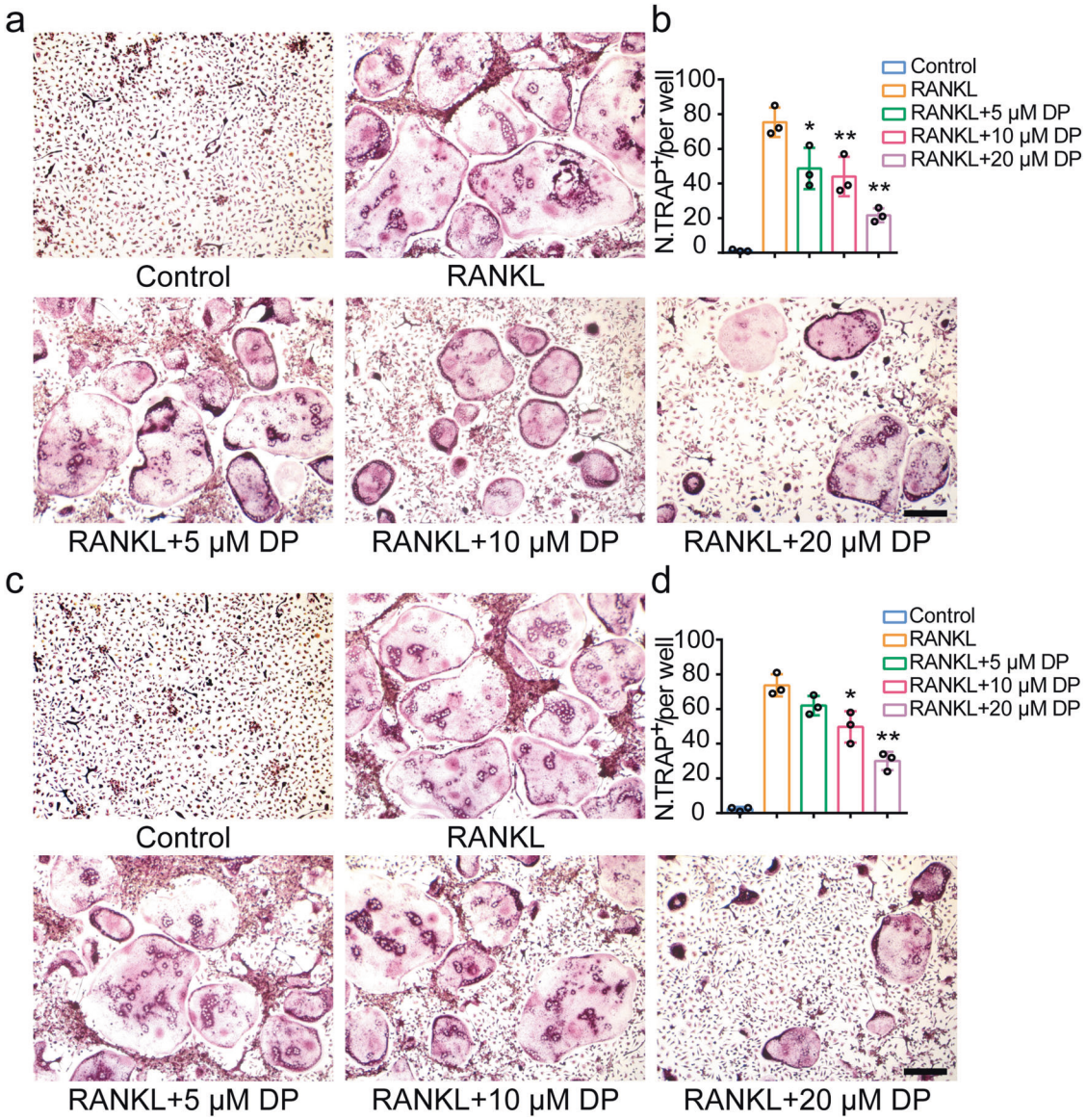

Fig. 5 **DP inhibits osteoclastogenesis in vitro. a**, **b** TRAP staining (**a**) and quantitative analysis (**b**) of osteoclasts induced from BMMCs. BMMCs were cultured with or without M-CSF and RANKL, treated with incremental levels of DP (5, 10, and 20 μM). Scale bar = 200 μm. **c**, **d** TRAP staining (**c**) and quantitative analysis (**d**) of osteoclasts induced from RAW264.7 cells. RAW264.7 cells cultured with or without RANKL, treated with various levels of DP (5, 10, and 20 μM). Scale bar = 200 μm. *$P < 0.05$ and **$P < 0.01$ compared with RANKL group.

20 μM, fewer multi-nuclear osteoclasts could be induced. Taken together, these results indicate that DP hampers osteoclastogenesis in vitro.

DP impairs osteoclast fusion by inhibiting the RANKL-induced ERK/c-fos/NFATc1 pathway

To gain insight into the mechanisms involved in the effect of DP, we examined in which stage DP had an inhibitory effect on osteoclastogenesis. After RAW264.7 cells were induced with RANKL, cellular double fluorescence assays were conducted in which cell nuclei were stained with Hoechst and cell membrane dye was labeled with Dil [49]. We found that the RANKL-induced cell membrane merge rate was significantly reduced in response to DP treatment (Fig. 6a, b). Therefore, we hypothesized that DP could inhibit osteoclast fusion. DC-STAMP [50] and Atp6v0d2 [51] are two critical modulators responsible for osteoclast fusion. NFATc1 and c-fos are regulated by the ERK signaling pathway and are required for osteoclast fusion by upregulating expression of DC-STAMP and Atp6v0d2 [52–54]. Immunofluorescence staining showed that DP dramatically blunted NFATc1 nuclear translocation after RANKL induction (Fig. 6c). Moreover, Western blotting indicated that expression levels of DC-STAMP and Atp6v0d2 and p-ERK, c-fos, and NFATc1 were significantly decreased by DP treatment. To gain further insight into the mechanisms underlying the effect of DP on the ERK/c-fos/NFATc1 axis, we chose Ceramide C6 as a specific ERK1/2 activator as previously reported [55–57]. After activating ERK phosphorylation with Ceramide C6, we found that Ceramide C6 abolished the effect of DP on RANKL-mediated osteoclast fusion and NFATc1 translocation, as assessed by immunofluorescence staining (Fig. 6a–c). Western blotting verified that expression levels of p-ERK, c-fos, and NFATc1, as well as downstream factors (DC-STAMP and Atp6v0d2), were significantly restored in the Ceramide C6 group in relative to DP group (Fig. 6d). Taken together, these findings demonstrate that DP impedes

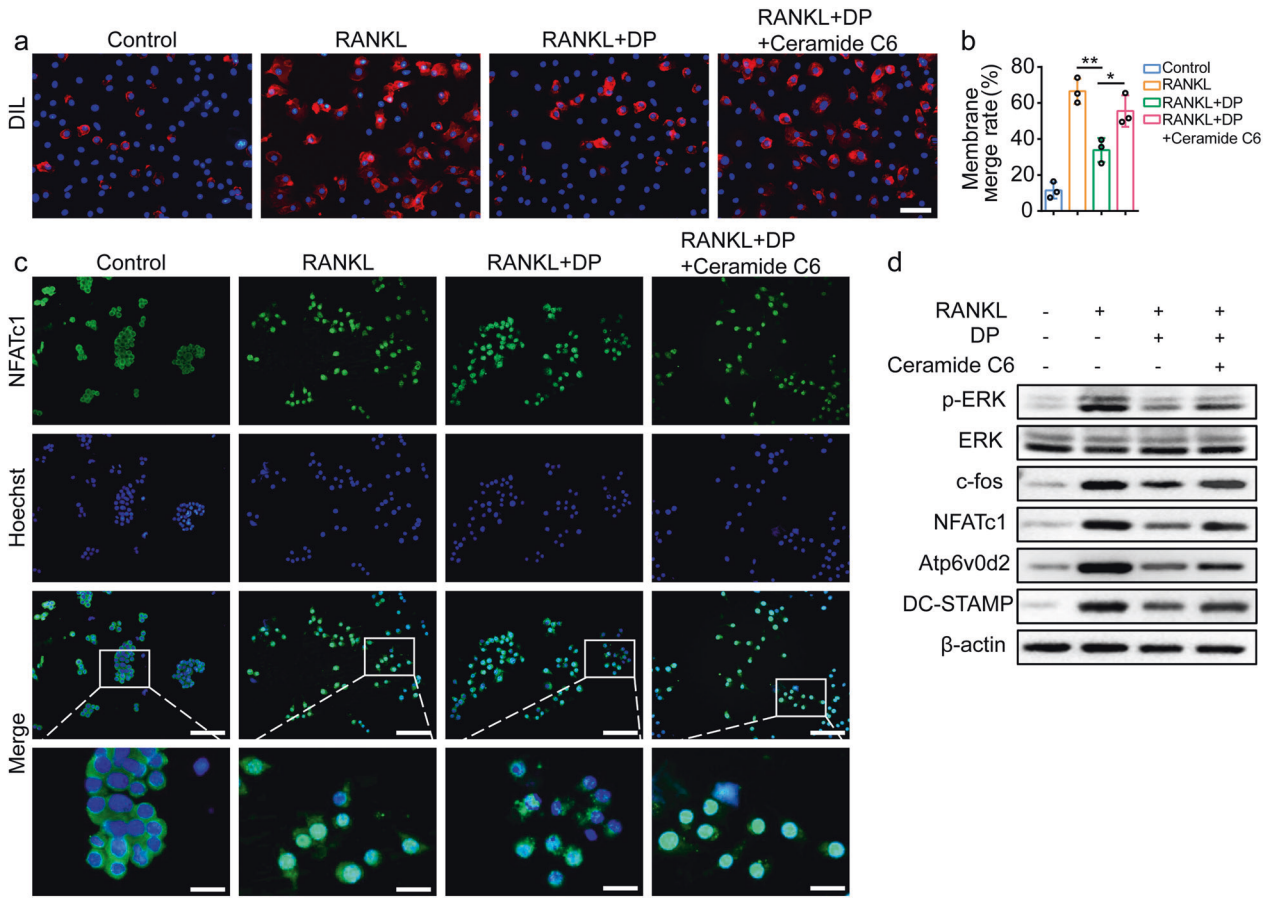

Fig. 6 DP blocks osteoclast fusion by suppressing RANKL-induced activation of ERK/c-fos/NFATc1 pathway. a Dil staining of cultured RAW264.7 cells induced for 3 days with or without RANKL, treated with DP (20 μM) in the presence or absence of Ceramide C6. Scale bar = 50 μm. **b** Quantification of membrane merge rate in four groups. **c** Immunofluorescence staining of NFATc1 nuclear translocation after RAW264.7 cells induced for 24 h with or without RANKL, treated with DP (20 μM) in the presence or absence of Ceramide C6. Scale bar = 25 μm (top). Scale bar = 6.25 μm (bottom). **d** Western blotting assay of p-ERK, ERK, c-fos, NFATc1, DC-STAMP, and Atp6v0d2 in cultured RAW264.7 cells induced with or without RANKL, treated with DP (20 μM) in the presence or absence of Ceramide C6. Control: RAW264.7 cells. RANKL: RAW264.7 cells stimulated with RANKL. RANKL+DP: RAW264.7 cells stimulated with RANKL, treated with DP (20 μM). RANKL+DP+Ceramide C6: RAW264.7 cells stimulated with RANKL, treated with DP (20 μM) and Ceramide C6. $^{*}P < 0.05$ and $^{**}P < 0.01$ compared with RANKL group or as denoted by bar.

osteoclast fusion by suppressing RANKL-mediated activation of the ERK/c-fos/NFATc1 axis.

DISCUSSION

In this research, we demonstrated that DP, which was identified from PN, effectively inhibited OA initiation and progression. Specifically, DP preserved the microarchitecture and decelerated abnormal angiogenesis in subchondral bone. DP also attenuated joint pain-related behavior by suppressing osteoclast-mediated sensory innervation in subchondral bone. Concomitantly, articular cartilage impairment was substantially ameliorated by DP. Mechanistically, this overactivated osteoclastogenesis in subchondral bone was notably abrogated by DP via inhibition of the ERK/c-fos/NFATc1 pathway (Fig. 7).

During adult bone remodeling, dynamic cross-talk between articular cartilage and subchondral bone guarantees joint homeostasis [58]. Increasing evidence indicates that microstructural alterations in subchondral bone caused by unstable mechanical loading on diarthrodial joints precede overlying cartilage degradation [20]. The overactivated subchondral bone remodeling rate triggered by elevated osteoclastic bone resorption is considered to be a leading pathological hallmark of OA, especially in the early stage [9, 59, 60]. Therefore, we propose that drugs targeting osteoclasts would be a promising therapeutic strategy for treating OA [17, 18, 24].

PN has long been used in the treatment of bone diseases, including promoting fracture healing [25], anti-inflammation [26], neuroprotection [27], and anti-osteoporosis [28]. In OA, PN has exerted potential therapeutic effects in progression prevention, pain relief, etc. [29, 30]. Nevertheless, the active components and mechanism remain unclear. According to our previous studies, 2D/BMMC/CMC/TOFMS acts as a bio-affinity scheme by which active constituents can be identified from complicated systems [31, 32]. The retention time of CMC hinges on the biological interaction between constituents and receptors on the BMMC membrane [33]. Obtained from this comprehensive system, the retention behavior focuses on DP identified from PN, presenting a potent affinity for BMMC membranes, suggesting that this active ingredient recognized from PN could be an available osteoclastogenesis inhibitor. Subsequently, an in vitro TRAP assay verified the anti-osteoclastogenic effect of DP in a dose-dependent manner.

Subchondral bone and articular cartilage constitute a osteochondral unit, which is distinctively designed to cushion mechanical loads and acclimatize to microenvironmental changes [6]. Early activated osteoclasts in subchondral bone are important in OA initiation. Under physiological conditions, few osteoclasts exist

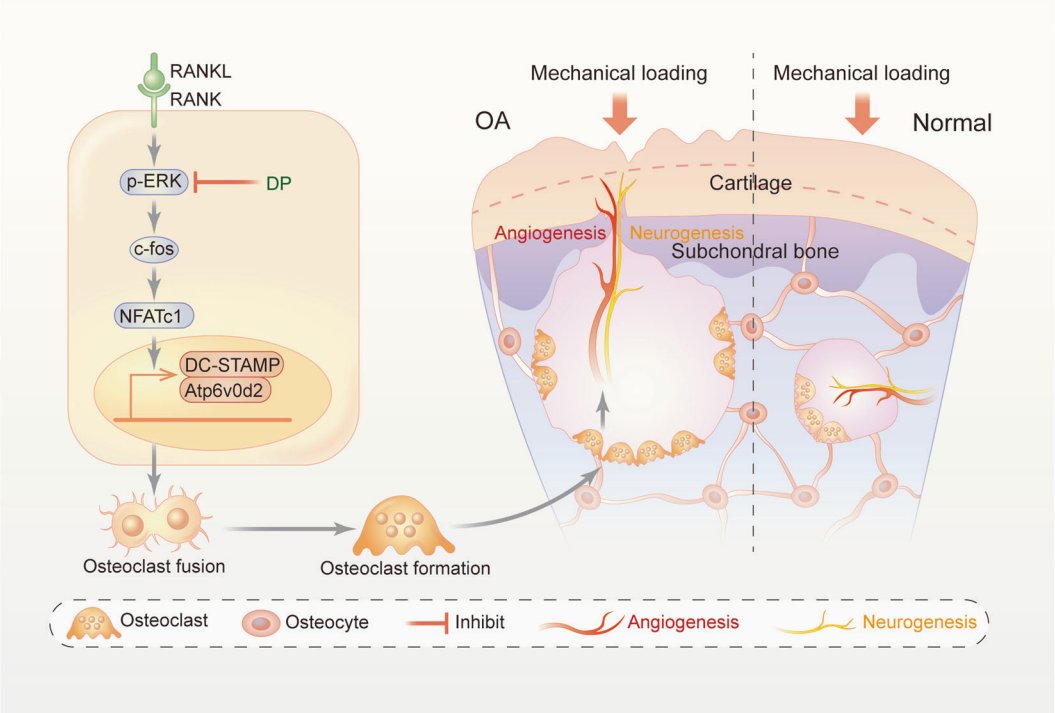

Fig. 7 Graphic abstract of the mechanisms. DP attenuates OA through inhibiting subchondral osteoclast fusion via suppressing ERK/c-fos/NFATc1 pathway.

in the subchondral bone area. After ACLT surgery, the number of TRAP-positive osteoclasts in subchondral bone was significantly increased and reached high levels at 2 weeks after ACLT, which alters the subchondral bone microstructure and gradually introduces blood vessels and sensory innervations towards overlying cartilage. In the onset of OA, osteoclastic bone resorption is aberrantly upregulated in subchondral bone due to a rapid bone turnover characterized by increased subchondral bone loss and enlarged bone marrow cavity with mild articular cartilage changes [16–18]. In the late stage of OA, osteogenesis takes the dominant role and the process of bone remodeling converts to enhanced bone formation, which is featured with increased SBP thickness and cancellous bone sclerosis. Despite the elevated bone volume, the enhanced bone turnover fails to improve the bone strength but causes the insufficient bone mineralization and reduced bone elastic modulus [6]. These pathological alterations ultimately lead to impaired biomechanical capacities of the subchondral bone, contributing to the following damage of overlying articular cartilage. Therefore, subchondral bone changes triggered by aberrant osteoclastogenesis precede the appearance of cartilage degeneration [10–12].

Overactivated osteoclastogenesis in subchondral bone in early OA leads to abnormal vascularization that exacerbates OA in a vicious circle. During OA, mounting vascularization from subchondral bone marrow infiltrates into osteochondral junctions through tunnels generated by osteoclastic bone resorption [61, 62]. Excessive angiogenesis contributes to osteogenesis and accelerates articular cartilage damage [47, 63]. Previous studies have confirmed that high expression levels of CD31 and EMCN ($CD31^{hi}EMCN^{hi}$) define H-type vessel coupling osteogenesis [64–67], and this special vessel subtype is a distinctive feature of OA [20]. In our study, we observed that colocalization of $CD31^{hi}EMCN^{hi}$ was elevated in subchondral bone in ACLT mice, as evaluated by immunofluorescence, while these changes were significantly diminished in the DP-treated group, suggesting that DP attenuates OA progression by preventing H-type vessel formation. We further investigated whether DP exhibits an inhibitory effect on MMP-2, which is released by endothelial cells and recognized as one of the membrane-associated neutral endopeptidases. MMP-2 functions as an angiogenesis promotor by degrading the structural extracellular matrix. In accordance with the results of $CD31^{hi}EMCN^{hi}$, DP reduced expression of MMP-2 in subchondral bone of ACLT group to the equivalent of that in sham group. These results demonstrate that DP blunts aberrant blood angiogenesis in subchondral bone with the abolishment of MMP-2-dependent tubular network formation.

Osteoclasts in subchondral bone introduce abnormal sensory nerve innervations, which leads to OA pain, a dominant and representative symptom. Osteoclasts could secrete netrin-1 and induces $CGRP^{+}$ sensory nerve innervation in subchondral bone. The abnormal CGRP sensory nerve results in hyperalgesia and OA pain [21, 23]. In this experiment, immunofluorescence staining revealed that the density of netrin-1 colocalized with TRAP in subchondral bone was increased in ACLT group consistent with the previous study [21]. DP treatment significantly inhibited $CGRP^{+}$ sensory nerve innervation in subchondral bone area after ACLT. In line with the results of immunofluorescence staining, behavioral changes assessed by the Von Frey test and plantar test in ACLT mice demonstrated the pain-relieving effect of DP.

For molecular mechanisms, we found that DP impeded osteoclast fusion. During osteoclastogenesis, mononucleated preosteoclasts derived from the monocyte/macrophage lineage fuse into multinucleated osteoclasts [68–70]. RANKL initiates the activation of extracellular signal-regulated kinase (ERK) [71], followed by sequential induction of c-fos and NFATc1, two essential transcription factors for osteoclast fusion [72, 73]. NFATc1 migrates into the nucleus and binds the promoter sequence of DC-STAMP and Atp6v0d2, two central regulators for osteoclast fusion [50, 51]. We previously uncovered that Oroxylin A extracted from *Radix Scutellariae* using the 2D/BMMC/CMC/TOFMS technique revealed an anti-osteoclastogeneic effect through prevention of osteoclast fusion [74]. In this study, Dil staining indicated that DP interrupted osteoclastogenesis by inhibiting osteoclast fusion, which was rescued by an ERK activator (Ceramide C6). Next, we verified this finding by immunofluorescence staining of NFATc1

nuclear translocation and Western blotting of the ERK/c-fos/NFATc1 axis. DC-STAMP and Atp6v0d2 were remarkably down-regulated in response to DP intervention. Activation of ERK phosphorylation with Ceramide C6 led to increased NFATc1 nuclear translocation and reversed the expression levels of the DC-STAMP and Atp6v0d2.

To our knowledge, we reveal for the first time the role of DP in the treatment of OA. Further optimization and modification of DP would uncover more therapeutic alterations for OA treatment. DP represents a promising pharmacological candidate to prevent OA onset and progression.

ACKNOWLEDGEMENTS

This work was supported by the National Key Research and Development Plan (2018YFC2001500); National Natural Science Foundation of China (NSFC) Key Research Program in Aging (91749204); National Natural Science Foundation of China (81771491, 81871099, 81972254); and Shanghai Rising-Star Program (21QA1412000). We thank the Experimental Center of Changhai Hospital for providing experimental instruments and reagents. The technique of 2D/BMMC/CMC/TOFMS is supported by the School of Pharmacy of Naval Medical University. We appreciate the work of Dr Yan-qiu Gu for screening DP from PN.

AUTHOR CONTRIBUTIONS

CF, XC, and JCS designed the research. CF, JWG, YJW, XQL, and HZ performed the experiments. JC, YH, and YYJ analyzed the data. XC and JCS interpreted the data. CF wrote the original manuscript. XC reviewed and edited the manuscript. CF and XC finalized the manuscript.

ADDITIONAL INFORMATION

Supplementary information The online version contains supplementary material available at https://doi.org/10.1038/s41401-021-00747-9.

Competing interests: The authors declare no competing interests.

REFERENCES

1. Chen D, Shen J, Zhao W, Wang T, Han L, Hamilton JL, et al. Osteoarthritis: toward a comprehensive understanding of pathological mechanism. Bone Res. 2017;5:16044.
2. Hunter DJ, Bierma-Zeinstra S. Osteoarthritis. Lancet. 2019:393:1745–59.
3. Zhang Z, Huang C, Jiang Q, Zheng Y, Liu Y, Liu S, et al. Guidelines for the diagnosis and treatment of osteoarthritis in China (2019 edition). Ann Transl Med. 2020;8:1213.
4. Tang X, Wang S, Zhan S, Niu J, Tao K, Zhang Y, et al. The prevalence of symptomatic knee osteoarthritis in China: results from the China Health and Retirement Longitudinal Study. Arthritis Rheumatol. 2016;68:648–53.
5. Koff RS, Dart RC. Osteoarthritis of the knee. N Engl J Med. 2006;354:2508–9. author reply 9
6. Goldring SR, Goldring MB. Changes in the osteochondral unit during osteoarthritis: structure, function and cartilage-bone crosstalk. Nat Rev Rheumatol. 2016;12:632–44.
7. Latourte A, Kloppenburg M, Richette P. Emerging pharmaceutical therapies for osteoarthritis. Nat Rev Rheumatol. 2020;16:673–88.
8. Sun MM, Beier F, Ratneswaran A. Nuclear receptors as potential drug targets in osteoarthritis. Curr Opin Pharmacol. 2018;40:81–6.
9. Hu W, Chen Y, Dou C, Dong S. Microenvironment in subchondral bone: predominant regulator for the treatment of osteoarthritis. Ann Rheum Dis. 2020;80:413–22.
10. Goldring SR. Alterations in periarticular bone and cross talk between subchondral bone and articular cartilage in osteoarthritis. Ther Adv Musculoskelet Dis. 2012;4:249–58.
11. Burr DB, Gallant MA. Bone remodelling in osteoarthritis. Nat Rev Rheumatol. 2012;8:665–73.
12. Sharma AR, Jagga S, Lee SS, Nam JS. Interplay between cartilage and subchondral bone contributing to pathogenesis of osteoarthritis. Int J Mol Sci. 2013;14:19805–30.
13. Deveza LA, Loeser RF. Is osteoarthritis one disease or a collection of many? Rheumatology. 2018;57:iv34–iv42.
14. Hayami T, Pickarski M, Wesolowski GA, McLane J, Bone A, Destefano J, et al. The role of subchondral bone remodeling in osteoarthritis: reduction of cartilage degeneration and prevention of osteophyte formation by alendronate in the rat anterior cruciate ligament transection model. Arthritis Rheum. 2004;50:1193–206.
15. Xiong J, Onal M, Jilka RL, Weinstein RS, Manolagas SC, O'Brien CA. Matrix-embedded cells control osteoclast formation. Nat Med. 2011;17:1235–41.
16. Tateiwa D, Yoshikawa H, Kaito T. Cartilage and bone destruction in arthritis: pathogenesis and treatment strategy: a literature review. Cells. 2019;8:818.
17. Strassle BW, Mark L, Leventhal L, Piesla MJ, Jian Li X, Kennedy JD, et al. Inhibition of osteoclasts prevents cartilage loss and pain in a rat model of degenerative joint disease. Osteoarthr Cartil. 2010;18:1319–28.
18. Bultink IE, Lems WF. Osteoarthritis and osteoporosis: what is the overlap? Curr Rheumatol Rep. 2013;15:328.
19. Xie H, Cui Z, Wang L, Xia Z, Hu Y, Xian L, et al. PDGF-BB secreted by preosteoclasts induces angiogenesis during coupling with osteogenesis. Nat Med. 2014;20:1270–8.
20. Zhen G, Wen C, Jia X, Li Y, Crane JL, Mears SC, et al. Inhibition of TGF-β signaling in mesenchymal stem cells of subchondral bone attenuates osteoarthritis. Nat Med. 2013;19:704–12.
21. Zhu S, Zhu J, Zhen G, Hu Y, An S, Li Y, et al. Subchondral bone osteoclasts induce sensory innervation and osteoarthritis pain. J Clin Invest. 2019;129:1076–93.
22. Suri S, Gill SE, Massena de Camin S, Wilson D, McWilliams DF, Walsh DA. Neurovascular invasion at the osteochondral junction and in osteophytes in osteoarthritis. Ann Rheum Dis. 2007;66:1423–8.
23. Ni S, Ling Z, Wang X, Cao Y, Wu T, Deng R, et al. Sensory innervation in porous endplates by Netrin-1 from osteoclasts mediates PGE2-induced spinal hypersensitivity in mice. Nat Commun. 2019;10:5643.
24. Karsdal MA, Bay-Jensen AC, Lories RJ, Abramson S, Spector T, Pastoureau P, et al. The coupling of bone and cartilage turnover in osteoarthritis: opportunities for bone antiresorptives and anabolics as potential treatments? Ann Rheum Dis. 2014;73:336–48.
25. Peng LH, Ko CH, Siu SW, Koon CM, Yue GL, Cheng WH, et al. In vitro & in vivo assessment of a herbal formula used topically for bone fracture treatment. J Ethnopharmacol. 2010;131:282–9.
26. Zhou X, Razmovski-Naumovski V, Chang D, Li C, Kam A, Low M, et al. Synergistic effects of Danshen (Salvia Miltiorrhiza Radix et Rhizoma) and Sanqi (Notoginseng Radix et Rhizoma) combination in inhibiting inflammation mediators in RAW264.7 cells. BioMed Res Int. 2016;2016:5758195.
27. Meng L, Huang Q, Li X, Liang P, Li Y, Huang X, et al. Genes induced by *Panax notoginseng* in a rodent model of ischemia-reperfusion injury. J Immunol Res. 2020;2020:8873261.
28. Wenxi D, Shufang D, Xiaoling Y, Liming Y. *Panax notoginseng* saponins suppress radiation-induced osteoporosis by regulating bone formation and resorption. Phytomedicine. 2015;22:813–9.
29. Chang SH, Sung HC, Choi Y, Ko SY, Lee BE, Baek DH, et al. Suppressive effect of AIF, a water extract from three herbs, on collagen-induced arthritis in mice. Int Immunopharmacol. 2005;5:1365–72.
30. Park SH, Kim SK, Shin IH, Kim HG, Choe JY. Effects of AIF on knee osteoarthritis patients: double-blind, randomized placebo-controlled study. Korean J Physiol Pharmacol. 2009;13:33–7.
31. Chen X, Cao Y, Zhang H, Zhu Z, Liu M, Liu H, et al. Comparative normal/failing rat myocardium cell membrane chromatographic analysis system for screening specific components that counteract doxorubicin-induced heart failure from *Acontium carmichaeli*. Anal Chem. 2014;86:4748–57.
32. Gu Y, Chen X, Wang R, Wang S, Wang X, Zheng L, et al. Comparative two-dimensional HepG2 and L02/ cell membrane chromatography/C18/time-of-flight mass spectrometry for screening selective anti-hepatoma components from Scutellariae Radix. J Pharm Biomed Anal. 2019;164:550–6.
33. Gu Y, Chen X, Wang Y, Liu Y, Zheng L, Li X, et al. Development of 3-mercaptopropyltrimethoxysilane (MPTS)-modified bone marrow mononuclear cell membrane chromatography for screening anti-osteoporosis components from Scutellariae Radix. Acta Pharm Sin B. 2020;10:1856–65.
34. Glasson SS, Blanchet TJ, Morris EA. The surgical destabilization of the medial meniscus (DMM) model of osteoarthritis in the 129/SvEv mouse. Osteoarthr Cartil. 2007;15:1061–9.
35. Khorasani MS, Diko S, Hsia AW, Anderson MJ, Genetos DC, Haudenschild DR, et al. Effect of alendronate on post-traumatic osteoarthritis induced by anterior cruciate ligament rupture in mice. Arthritis Res Ther. 2015;17:30.
36. Zhu S, Chen K, Lan Y, Zhang N, Jiang R, Hu J. Alendronate protects against articular cartilage erosion by inhibiting subchondral bone loss in ovariectomized rats. Bone. 2013;53:340–9.
37. Siebelt M, Waarsing JH, Groen HC, Müller C, Koelewijn SJ, de Blois E, et al. Inhibited osteoclastic bone resorption through alendronate treatment in rats reduces severe osteoarthritis progression. Bone. 2014;66:163–70.

38. Yeon JT, Kim KJ, Choi SW, Moon SH, Park YS, Ryu BJ, et al. Anti-osteoclastogenic activity of praeruptorin A via inhibition of p38/Akt-c-Fos-NFATc1 signaling and PLCγ-independent Ca2+ oscillation. PloS One. 2014;9:e88974.
39. Cui Z, Crane J, Xie H, Jin X, Zhen G, Li C, et al. Halofuginone attenuates osteoarthritis by inhibition of TGF-β activity and H-type vessel formation in subchondral bone. Ann Rheum Dis. 2016;75:1714–21.
40. Glasson SS, Chambers MG, Van Den Berg WB, Little CB. The OARSI histopathology initiative—recommendations for histological assessments of osteoarthritis in the mouse. Osteoarthr Cartil. 2010;18:S17–23.
41. Wei JL, Fu W, Ding YJ, Hettinghouse A, Lendhey M, Schwarzkopf R, et al. Progranulin derivative Atsttrin protects against early osteoarthritis in mouse and rat models. Arthritis Res Ther. 2017;19:280.
42. Austin PJ, Wu A, Moalem-Taylor G. Chronic constriction of the sciatic nerve and pain hypersensitivity testing in rats. J Vis Exp. 2012: 3393.
43. Dixon WJ. Efficient analysis of experimental observations. Annu Rev Pharmacol Toxicol. 1980;20:441–62.
44. Hargreaves K, Dubner R, Brown F, Flores C, Joris J. A new and sensitive method for measuring thermal nociception in cutaneous hyperalgesia. Pain. 1988;32:77–88.
45. Ahmad Dar A, Sangwan PL, Kumar A. Chromatography: an important tool for drug discovery. J Sep Sci. 2020;43:105–19.
46. Ding M, Danielsen CC, Hvid I. The effects of bone remodeling inhibition by alendronate on three-dimensional microarchitecture of subchondral bone tissues in guinea pig primary osteoarthrosis. Calcif Tissue Int. 2008;82:77–86.
47. Wang Y, Xu J, Zhang X, Wang C, Huang Y, Dai K, et al. TNF-α-induced LRG1 promotes angiogenesis and mesenchymal stem cell migration in the subchondral bone during osteoarthritis. Cell Death Dis. 2017;8:e2715.
48. Chen Q, Jin M, Yang F, Zhu J, Xiao Q, Zhang L. Matrix metalloproteinases: inflammatory regulators of cell behaviors in vascular formation and remodeling. Mediators Inflamm. 2013;2013:928315.
49. Li B, Yu F, Wu F, Wang K, Lou F, Zhang D, et al. Visual osteoclast fusion via a fluorescence method. Sci Rep. 2018;8:10184.
50. Yagi M, Miyamoto T, Sawatani Y, Iwamoto K, Hosogane N, Fujita N, et al. DC-STAMP is essential for cell-cell fusion in osteoclasts and foreign body giant cells. J Exp Med. 2005;202:345–51.
51. Lee SH, Rho J, Jeong D, Sul JY, Kim T, Kim N, et al. v-ATPase V0 subunit d2-deficient mice exhibit impaired osteoclast fusion and increased bone formation. Nat Med. 2006;12:1403–9.
52. Nakamura I, Takahashi N, Jimi E, Udagawa N, Suda T. Regulation of osteoclast function. Mod Rheumatol. 2012;22:167–77.
53. Kim K, Lee SH, Ha Kim J, Choi Y, Kim N. NFATc1 induces osteoclast fusion via up-regulation of Atp6v0d2 and the dendritic cell-specific transmembrane protein (DC-STAMP). Mol Endocrinol. 2008;22:176–85.
54. Lee MS, Kim HS, Yeon JT, Choi SW, Chun CH, Kwak HB, et al. GM-CSF regulates fusion of mononuclear osteoclasts into bone-resorbing osteoclasts by activating the Ras/ERK pathway. J Immunol. 1950;2009:3390–9.
55. Müller G, Storz P, Bourteele S, Döppler H, Pfizenmaier K, Mischak H, et al. Regulation of Raf-1 kinase by TNF via its second messenger ceramide and cross-talk with mitogenic signalling. EMBO J. 1998;17:732–42.
56. Yan J, Zuo G, Sherchan P, Huang L, Ocak U, Xu W, et al. CCR1 activation promotes neuroinflammation through CCR1/TPR1/ERK1/2 signaling pathway after intracerebral hemorrhage in mice. Neurotherapeutics. 2020;17:1170–83.
57. Yang A, Suh WI, Kang NK, Lee B, Chang YK. MAPK/ERK and JNK pathways regulate lipid synthesis and cell growth of Chlamydomonas reinhardtii under osmotic stress, respectively. Sci Rep. 2018;8:13857.
58. Lories RJ, Luyten FP. The bone-cartilage unit in osteoarthritis. Nat Rev Rheumatol. 2011;7:43–9.
59. Zhen G, Cao X. Targeting TGFbeta signaling in subchondral bone and articular cartilage homeostasis. Trends Pharmacol Sci. 2014;35:227–36.
60. Li Y, Mu W, Xu B, Ren J, Wahafu T, Wuermanbieke S, et al. Artesunate, an anti-malaria agent, attenuates experimental osteoarthritis by inhibiting bone resorption and CD31(hi)Emcn(hi) vessel formation in subchondral bone. Front Pharmacol. 2019;10:685.
61. Cui Z, Xu C, Li X, Song J, Yu B. Treatment with recombinant lubricin attenuates osteoarthritis by positive feedback loop between articular cartilage and subchondral bone in ovariectomized rats. Bone. 2015;74:37–47.
62. Donell S. Subchondral bone remodelling in osteoarthritis. EFORT Open Rev. 2019;4:221–9.
63. Guiducci S, Manetti M, Romano E, Mazzanti B, Ceccarelli C, Dal Pozzo S, et al. Bone marrow-derived mesenchymal stem cells from early diffuse systemic sclerosis exhibit a paracrine machinery and stimulate angiogenesis in vitro. Ann Rheum Dis. 2011;70:2011–21.
64. Kusumbe AP, Ramasamy SK, Adams RH. Coupling of angiogenesis and osteogenesis by a specific vessel subtype in bone. Nature. 2014;507:323–8.
65. Mapp PI, Walsh DA. Mechanisms and targets of angiogenesis and nerve growth in osteoarthritis. Nat Rev Rheumatol. 2012;8:390–8.
66. Aso K, Shahtaheri SM, Hill R, Wilson D, McWilliams DF, Nwosu LN, et al. Contribution of nerves within osteochondral channels to osteoarthritis knee pain in humans and rats. Osteoarthr Cartil. 2020;28:1245–54.
67. Walsh DA, Mapp PI, Kelly S. Calcitonin gene-related peptide in the joint: contributions to pain and inflammation. Br J Clin Pharmacol. 2015;80:965–78.
68. Helming L, Gordon S. Molecular mediators of macrophage fusion. Trends Cell Biol. 2009;19:514–22.
69. Pereira M, Petretto E, Gordon S, Bassett JHD, Williams GR, Behmoaras J. Common signalling pathways in macrophage and osteoclast multinucleation. J Cell Sci. 2018;131:jcs216267.
70. Kodama J, Kaito T. Osteoclast multinucleation: review of current literature. Int J Mol Sci. 2020;21:5685.
71. Boyle WJ, Simonet WS, Lacey DL. Osteoclast differentiation and activation. Nature. 2003;423:337–42.
72. Grigoriadis AE, Wang ZQ, Cecchini MG, Hofstetter W, Felix R, Fleisch HA, et al. c-Fos: a key regulator of osteoclast-macrophage lineage determination and bone remodeling. Science. 1994;266:443–8.
73. Takayanagi H. The role of NFAT in osteoclast formation. Ann N Y Acad Sci. 2007;1116:227–37.
74. Li X, Wang L, Huang B, Gu Y, Luo Y, Zhi X, et al. Targeting actin-bundling protein *L*-plastin as an anabolic therapy for bone loss. Sci Adv. 2020;6:eabb7135.